Article

Ne–NH van der Waals Tetramer: Rotational Spectra and ab Initio Study of the Microsolvation of NH with Rare Gas Atoms

Jennifer van Wijngaarden, and Wolfgang Jger

J. Am. Chem. Soc., **2003**, 125 (47), 14631-14641• DOI: 10.1021/ja035252p • Publication Date (Web): 30 October 2003

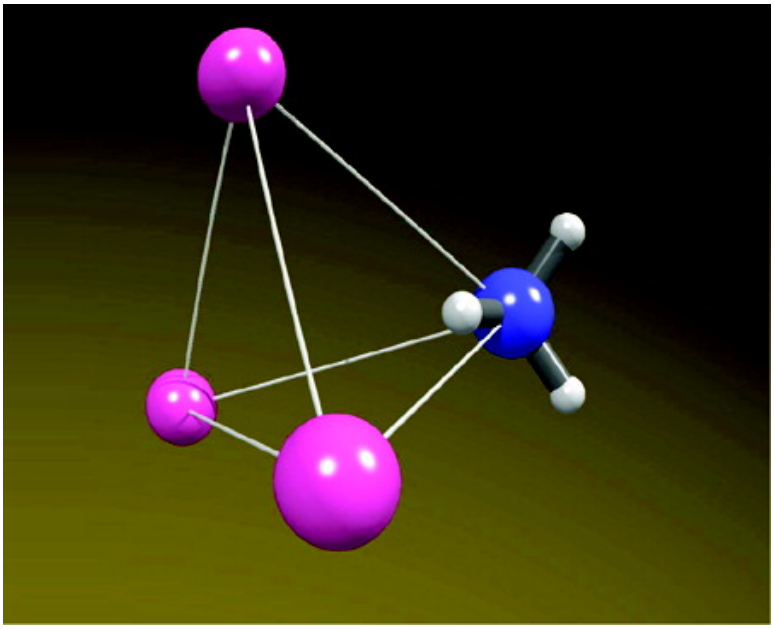

J|A|C|S
ARTICLES
Published on Web 10/30/2003

Ne_3-NH_3 van der Waals Tetramer: Rotational Spectra and ab Initio Study of the Microsolvation of NH_3 with Rare Gas Atoms

Jennifer van Wijngaarden† and Wolfgang Jäger*

Contribution from the Department of Chemistry, University of Alberta, Edmonton, Alberta, Canada T6G 2G2

Received March 20, 2003; E-mail: wolfgang.jaeger@ualberta.ca

Abstract: Microwave rotational spectra of eleven isotopomers of the Ne_3-NH_3 van der Waals tetramer were measured using a pulsed jet, Balle−Flygare type Fourier transform microwave spectrometer. The transitions measured fall between 4 and 17 GHz and correspond to the ground internal rotor state of the weakly bound complex. The $^{20}Ne_3$- and $^{22}Ne_3$-containing species are symmetric top molecules while the mixed $^{20}Ne_2{}^{22}Ne$- and $^{20}Ne^{22}Ne_2$-isotopomers are asymmetric tops. For each of the deuterium-containing isotopomers, a tunneling splitting was observed due to the inversion of NH_3 within the tetramer. The ^{14}N nuclear quadrupole hyperfine structures were resolved and included in the spectroscopic fits of the various isotopomers. The rotational constants obtained from the fits were used to estimate the van der Waals bond lengths of the tetramer while the ^{14}N nuclear quadrupole coupling contants and the observed inversion tunneling splittings provided information about the internal dynamics of the NH_3 moiety. The experimental results were complemented by the construction of three ab initio potential energy surfaces [CCSD(T)] for the Ne_3-NH_3 complex, each corresponding to a different internal geometry of NH_3 ($\angle HNH = 106.67°$, $\angle HNH = 113.34°$, and $\angle HNH = 120.00°$). The topologies of the surfaces are related to the structures and dynamics of the tetramer. Extensive comparisons are made between the results obtained for the Ne_3-NH_3 tetramer in this work and previous experimental and ab initio studies of related Rg_n-NH_3 van der Waals clusters.

1. Introduction

It is well established that the chemical and physical properties of condensed phases are fundamentally dependent on weak intermolecular interactions. To achieve a thorough understanding of the behavior of a substance, it is necessary to first probe its properties on the microscopic scale. Information regarding isolated intermolecular interactions is available via high resolution spectroscopic studies of van der Waals complexes produced in a supersonic jet expansion. The spectra provide accurate details concerning the structures and dynamics of these weakly bound complexes on the microscopic level and thus play a crucial role in the development and refinement of theoretical models that characterize weak intermolecular interactions.

For weakly bound complexes consisting of more than two substituents, it is necessary to identify nonadditive contributions to the intermolecular interaction energy. van der Waals molecules that contain a number of rare gas (Rg) atoms bound to one molecule are particularly attractive candidates for deducing the importance of nonadditive effects since many Rg−Rg and Rg−molecule binary potentials have been well-characterized. This allows the nonadditive contributions to the intermolecular interaction energy to be isolated in principle. With molecular beam techniques, van der Waals clusters of different sizes can be generated and thus Rg_n−molecule systems are good prototypes for investigating solvation on the molecular level. In particular, Rg atoms are chosen as the ideal solvent for such investigations since they serve as structureless probes of weak interactions with the molecule of interest. The ability to produce a range of differently sized Rg_n−molecule microclusters thus affords the opportunity to observe, on the microscopic level, how both the structural and dynamical properties of weakly bound complexes evolve as successive Rg atoms are added. For comparison, the molecule of interest can be spectroscopically probed in cryogenic Rg matrixes which provides a definition of the bulk limit that the Rg_n−molecule clusters approach.[1] In this respect, van der Waals clusters have the potential to bridge the gap between isolated molecules and condensed phases. As an example, it has recently been demonstrated, for the case of superfluidity, how trends in spectroscopic constants from high resolution spectroscopic studies of clusters in the intermediate size regime can trace the onset of a phenomenon that is formally macroscopic in nature.[2]

Weak interactions that involve NH_3 are of particular interest due to the fundamental importance of NH_3 in a variety of industrial and commercial chemical processes such as petroleum refining, metallurgy, semiconductor manufacturing, and the production of goods such as explosives, insecticides, and nylon. Ammonia also has the distinction of being the first polyatomic

† Present address: Universität Basel, Institut für Physikalische Chemie, Klingelbergstr. 80, CH-4056 Basel, Switzerland.

(1) Bačić, Z. *Theory of Atomic and Molecular Clusters*; Jellinek, J., Ed.; Springer-Verlag, Berlin, 1999.
(2) Tang, J.; Xu, Y.; McKellar, A. R. W.; Jäger, W. *Science* **2002**, *297*, 2030.

molecule found in space[3] and is believed to play an important role in the chemistry of interstellar media.[4] Since the reactivity of NH_3 depends on its interactions with other molecules, a precise knowledge of weak interactions with NH_3 is integral to the understanding of these processes on the molecular level. It is not surprising, therefore, that a number of NH_3-containing van der Waals dimers, such as NH_3-NH_3,[5] NH_3-H_2O,[6] NH_3-HCN,[7] NH_3-CH_3OH,[8] and NH_3-N_2O,[9] among many others, have been the subject of spectroscopic study over the past 20 years.

The $Ar-NH_3$ complex, in particular, has been the subject of numerous spectroscopic[10−12] and theoretical investigations.[13] It is regarded as a prototype system for modeling the coupling of intermolecular and intramolecular modes in weakly bound complexes. This is because the NH_3 subunit undergoes large amplitude internal rotation and inversion motions within the complex leading to the spectroscopic observation of several tunneling states. Of special interest are the deuterated isotopomers (ND_3, ND_2H, and NDH_2) since, for these species, an inversion tunneling splitting can be observed in the ground internal rotor states of the complexes.[14,15] For the normal NH_3-containing complexes, the symmetric inversion component has a nuclear spin statistical weight of zero and cannot be observed.

To date, microwave spectra have been recorded for a series of $Rg-NH_3$ dimers (Rg = Ne,[16] Ar,[11,14] Kr[17]) in an effort to determine the effect of the Rg binding partner's size and polarizability on the internal dynamics of NH_3 in weakly bound complexes. In these studies, analysis of the nuclear quadrupole hyperfine structures arising from the quadrupolar ^{14}N nucleus (nuclear spin quantum number $I = 1$) have provided information about the internal rotation of NH_3 since the observed splitting patterns are intrinsically linked to the orientation and internal rotor dynamics of NH_3 within these complexes. Second, the inversion tunneling splittings observed for the deuterated species have enabled comparisons of the NH_3 inversion motion in different Rg enviroments. The dimer investigations were later extended to the Rg_2-NH_3 trimer (Rg = Ne,[18] Ar)[19] systems to probe the effect of larger Rg clusters on these internal motions and to identify the importance of three-body nonadditive effects in NH_3-containing complexes. More recently, a microwave spectroscopic investigation of the Ar_3-NH_3 tetramer[20] has been reported. The spectra revealed that the large amplitude internal rotation and inversion motions of NH_3 are still present in the quaternary complex. In fact, the magnitudes of these internal motions remain large enough that the observed spectra of Ar_3-NH_3 resembled those of a symmetric top since the dipole moment of the NH_3 monomer is effectively averaged out.

A similar study of the Ne_3-NH_3 tetramer promises to reveal further information concerning the microsolvation of NH_3 with Rg atoms, since the properties of the Rg binding partner have a profound influence on the energetics of the complex and lead to spectroscopically detectable differences in the structures and dynamics of these microclusters. Furthermore, the Ne_3-NH_3 tetramer is more amenable to ab initio study than the Ar analogue since the basis sets required to adequately describe Ne atoms are smaller and thus more computationally manageable. The construction of an ab initio potential energy surface of Ne_3-NH_3 will provide a useful comparison with the previously published surfaces of $Ne-NH_3$[16] and Ne_2-NH_3[18] which proved to be quite complementary with their respective microwave spectra. In this respect, the combined microwave spectroscopic and ab initio study of Ne_3-NH_3 will close a crucial gap in the investigation of the structures and dynamics of the Rg_n-NH_3 ($n = 1, 2, 3$) family.

This paper describes the first high-resolution microwave spectra of eleven isotopomers of Ne_3-NH_3. The spectra are assigned to the ground internal rotor state of the quaternary complex which correlates with the $j = 0$, $k = 0$ free rotor state of NH_3. The rotational constants, ^{14}N nuclear quadrupole hyperfine structures, and inversion tunneling splittings are analyzed and discussed in terms of the structures and dynamics of the tetramer in relation to the previously reported $Rg-NH_3$ dimers, Rg_2-NH_3 trimers, and the Ar_3-NH_3 tetramer. Furthermore, three ab initio potential energy surfaces were constructed for Ne_3-NH_3 at the CCSD(T) level of theory. The theoretical results are compared with the observed tetramer spectra and with the potential energy surfaces of $Ne-NH_3$ and Ne_2-NH_3 described previously.

2. Experimental Method

Rotational spectra of the Ne_3-NH_3 tetramer were recorded between 4 and 17 GHz using a pulsed jet Balle−Flygare[21] type Fourier transform microwave spectrometer that has been previously described.[22,23] It was necessary, due to the small dipole moments of the Ne_3-NH_3 tetramers, to add a microwave power amplifier to the excitation branch of the instrument in order to achieve the $\pi/2$ excitation pulse condition. The complexes were produced in a molecular beam expansion of a gas mixture through a pulsed nozzle with an orifice diameter of 0.8 mm (General Valve Corp., Series 9). The supersonic jet expansion runs

(3) Cheung, A. C.; Rank, D. M.; Townes, C. H.; Thornton, D. D.; Welch, W. J. *Phys. Rev. Lett.* **1968**, *21*, 1701.
(4) Roueff, E.; Time, S.; Coudert, L. H.; Pineau des Forets, G.; Falgraone, E.; Gerin, M. *Astron. Astrophys.* **2000**, *354*, L63. Peng, Y.; Vogel, S. N.; Carlstrom, J. E. *Astrophys. J.* **1993**, *418*, 255.
(5) Karyakin, E. N.; Fraser, G. T.; Loeser, J. G.; Saykally, R. J. *J. Chem. Phys.* **1999**, *110*, 9555 and references therein.
(6) Fraser, G. T.; Suenram, R. D. *J. Chem. Phys.* **1992**, *96*, 7287 and references therein.
(7) Fraser, G. T.; Leopold, K. R.; Nelson, D. D., Jr.; Tung, A.; Klemperer, W. *J. Chem. Phys.* **1986**, *80*, 3073.
(8) Fraser, G. T.; Suenram, R. D.; Lovas, F. J.; Stevens, W. J. *Chem. Phys.* **1988**, *125*, 35.
(9) Ott, M. E.; Leopold, K. R. *J. Chem. Phys. A.* **1999**, *103*, 1322.
(10) Schmuttenmaer, C. A.; Loeser, J. G.; Saykally, R. J. *J. Chem. Phys.* **1994**, *101*, 139. Grushow, A.; Burns, W. A.; Reeve, S. W.; Dvorak, M. A.; Leopold, K. R. *J. Chem. Phys.* **1994**, *100*, 2413. Schmuttenmaer, C. A.; Cohen, R. C.; Loeser, J. G.; Saykally, R. J. *J. Chem. Phys.* **1991**, *95*, 9. Fraser, G. T.; Pine, A. S.; Kreiner, W. A. *J. Chem. Phys.* **1991**, *94*, 7061. Gwo, D.-H.; Havenith, M.; Busarow, K. L.; Cohen, R. C.; Schmuttenmaer, C. A.; Saykally, R. J. *Mol. Phys.* **1990**, *71*, 453. Bizzarri, A.; Heijmen, B.; Stolte, S.; Reuss, J. *Z. Physica D* **1988**, *10*, 291.
(11) Nelson, D. D., Jr.; Fraser, G. T.; Peterson, K. I.; Zhao, K.; Klemperer, W.; Lovas, F. J.; Suenram, R. D. *J. Chem. Phys.* **1986**, *85*, 5512. Fraser, G. T.; Nelson, D. D., Jr.; Charo, A.; Klemperer, W. *J. Chem. Phys.* **1985**, *82*, 2535.
(12) Zwart, E.; Linnartz, H.; Meerts, W. L.; Fraser, G. T.; Nelson, D. D., Jr.; Klemperer, W. *J. Chem. Phys.* **1991**, *95*, 793.
(13) Schmuttenmaer, C. A.; Cohen, R. C.; Saykally, R. J. *J. Chem. Phys.* **1994**, *101*, 146. Tao, F.-M.; Klemperer, W. *J. Chem. Phys.* **1994**, *101*, 1129. van Bladel, J. W. I.; van der Avoird, A.; Wormer, P. E. S. *Chem. Phys.* **1992**, *165*, 47; *ibid. J. Chem. Phys.* **1991**, *95*, 5414; *ibid. J. Chem. Phys.* **1991**, *94*, 501. Bulski, F.; Wormer, P. E. S.; van der Avoird, A. *J. Chem. Phys.* **1991**, *94*, 491. Chałasiński, G.; Cybulski, S. M.; Szczęśniak, M. M.; Scheiner, S. *J. Chem. Phys.* **1989**, *91*, 7809.
(14) van Wijngaarden, J.; Jäger, W. *J. Chem. Phys.* **2001**, *114*, 3968.
(15) Melnik, D. G.; Gopalakrishnan, S.; Miller, T. A.; De Lucia, F.; Belov. S. *J. Chem. Phys.* **2001**, *114*, 6100.
(16) van Wijngaarden, J.; Jäger, W. *J. Chem. Phys.* **2001**, *115*, 6504.
(17) van Wijngaarden, J.; Jäger, W. *Mol. Phys.* **2001**, *99*, 1215.
(18) van Wijngaarden, J.; Jäger, W. *Chem. Phys.* **2002**, *283*, 29.
(19) van Wijngaarden, J.; Jäger, W. *Phys. Chem. Chem. Phys.* **2002**, *4*, 4883.
(20) van Wijngaarden, J.; Jäger, W. *J. Chem. Phys.* **2002**, *116*, 2379.
(21) Balle, T. J.; Flygare, W. H. *Rev. Sci. Instrum.* **1981**, *52*, 33.
(22) Xu, Y.; Jäger, W. *J. Chem. Phys.* **1997**, *106*, 7968.
(23) Grabow, J.-U.; Stahl, W. *Z. Naturforsch., A: Phys. Sci.* **1990**, *45*, 1043.

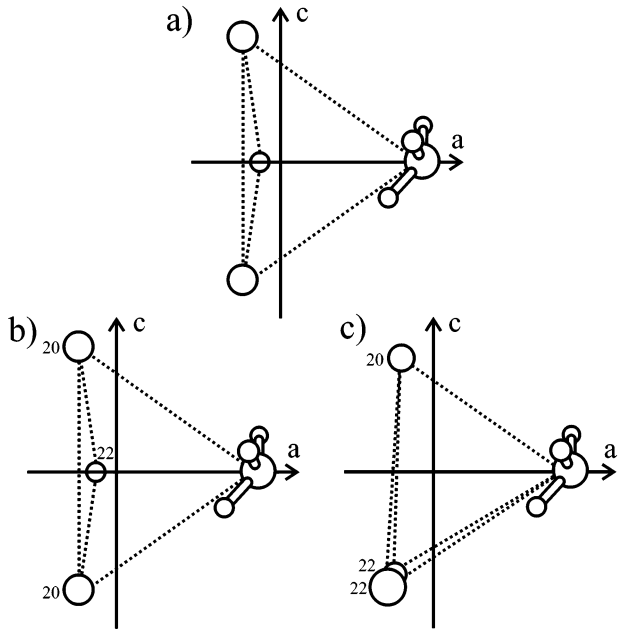

Figure 1. Geometries of the Ne_3-NH_3 isotopomers in the principal inertial axis system. (a) The ^{20}Ne- and ^{22}Ne-containing Ne_3Ne_3 isotopomers are prolate symmetric tops. (b) The $^{20}Ne_2{}^{22}Ne$- and (c) $^{20}Ne^{22}Ne_2$-containing isotopomers are asymmetric tops.

parallel to the axis of the microwave cavity, and consequently, all recorded spectra appear Doppler doubled.

The gas sample was prepared at room temperature and consisted of approximately 0.5% NH_3 in Ne to backing pressures of 12 atm. The ^{22}Ne-containing species were measured in natural abundance (8.82% ^{22}Ne) while isotopically enriched samples were necessary to record the spectra of the ^{15}N- (Cambridge Isotopes: 98% $^{15}NH_3$) and deuterium-containing (Cambridge Isotopes: 99% ND_3) isotopomers. The intensity of the ND_2H- and NDH_2-containing species increased dramatically after the ND_3-containing gas mixture was left in the sample system for several hours.

3. Spectral Search and Assignment

Although several Ar_3-molecule tetramers have been studied by microwave spectroscopy,[24−28] only one Ne_3-containing van der Waals tetramer, Ne_3Ar,[28] has been previously investigated. The Ne_3Ar tetramer is a prolate symmetric top, and the Ne−Ne and Ne−Ar bond lengths were reported to be 0.01 and 0.006 Å shorter than the respective dimer values. The Ne_3-NH_3 complex was similarly predicted to be a prolate symmetric top. The presence of ^{22}Ne in 8.82% natural abundance allows the production of four different isotopomers of Ne_3-NH_3 before ^{15}N or deuterium substitution is considered. These isotopomers were expected to display very distinct spectra. The $^{20}Ne_3$- and $^{22}Ne_3$-containing species are prolate symmetric tops as shown in Figure 1 a in the principal inertial axis system. The $^{20}Ne_2{}^{22}$-Ne- and $^{20}Ne^{22}Ne_2$-containing isotopomers are asymmetric tops as depicted in Figure 1b and c, respectively. The $^{20}Ne_2{}^{22}Ne$-containing species has nonzero dipole moment contributions along the *a*- and *b*-axes, and both *a*- and *b*-type rotational spectra were anticipated. The $^{20}Ne^{22}Ne_2-NH_3$ complex has nonzero dipole moment contributions along the *a*- and *c*-axes, and the expected transitions were *a*- and *c*-type. The nuclear spin statistical weights of the various symmetric rotor and asymmetric rotor energy levels were determined by molecular symmetry group analyses[29] of each isotopomer.

Earlier microwave studies of the $Rg-NH_3$ (Rg = Ne,[16] ^{16}Kr[17]) dimers, Rg_2-NH_3 (Rg = Ne,[18] Ar[19]) trimers, and the Ar_3-NH_3 tetramer demonstrated that the internal rotation and inversion of the NH_3 subunit is not significantly hindered when bound to one, two, or three Rg atoms. These large amplitude motions result in the appearance of metastable internal rotor and inversion tunneling states in the spectra of certain isotopomers. Analysis of the spectra of these tunneling states provides information about the dynamics of NH_3 in the various Rg_n cluster environments. Similar large amplitude internal motions were expected for the various isotopomers of Ne_3-NH_3, and the predicted spin statistical weights of the metastable tunneling states are discussed below.[29]

The states of Ne_3-NH_3 are labeled according to the free rotor state of NH_3 that they correlate with. For NH_3 and ND_3, the symmetric top quantum numbers j_k are used while asymmetric top labels ($j_{k_a k_c}$) are used for the ND_2H and NDH_2 containing isotopomers. The addition of a Greek letter before the free rotor label describes the projection (*K*) of *j* onto the intermolecular *a*-axis and is Σ for $K = 0$, Π for $K = 1$, and so forth. An additional subscript "s" or "a" may be included to describe the symmetry of the NH_3 inversion wave function depending on whether it is symmetric or antisymmetric, respectively.

3.1. $^{20}Ne_3-NH_3$, $^{22}Ne_3-NH_3$, $^{20}Ne_3-{}^{15}NH_3$, and $^{22}Ne_3-{}^{15}NH_3$. The prolate symmetric top complexes containing NH_3 or $^{15}NH_3$ belong to the G_{72} molecular symmetry group.[29] The analysis was simplified by using the smaller G_{36} group since the internal motion corresponding to a flip of the Ne_3 ring (thus changing its handedness relative to the NH_3 subunit) was not deemed feasible for the purposes of this experiment. The symmetries of the various components of the wave function are summarized in Table 1 and are explained in more detail for Ar_3-NH_3.[20] From the analysis, it becomes apparent that, for the ground internal rotor state of the Ne_3-NH_3 complex, all rotational levels corresponding to the symmetric inversion component, $\Sigma 0_{0s}$, have a nuclear spin statistical weight of zero. Thus, no rotational transitions are observed for this state. For the antisymmetric inversion component, $\Sigma 0_{0a}$, only levels with $K = 3n$ ($n = 0, 1, 2, ...$) have nonzero spin statistical weights and the rotational spectrum will consist of transitions within these K-stacks. Energy levels with $K \neq 3n$ have nuclear spin statistical weights of zero. In comparison to oblate symmetric tops such as Ar_3-NH_3, the $K = 3$ levels are shifted to a higher energy than the $K = 0$ levels in a prolate symmetric top and the D_{JK} constant is positive.[30]

Assuming dimer values for the Ne−Ne (3.29 Å)[28] and Ne−NH_3 (3.723 Å)[16] bond lengths, the *B* rotational constant of $^{20}Ne_3-NH_3$ was predicted within 2 MHz of the experimental value. In total, four rotational transitions were measured and assigned to the $\Sigma 0_{0a}$ state of each of the following isoto-

(24) Gutowsky, H. S.; Klots, T. D.; Chuang, C.; Keen, J. D.; Schmuttenmaer, C. A.; Emilsson, T. *J. Am. Chem. Soc.* **1985**, *107*, 7174. Klots, T. D.; Gutowsky, H. S. *J. Am. Chem. Soc.* **1987**, *109*, 5633.
(25) Klots, T. D.; Ruoff, R. S.; Chuang, C.; Emilsson, T.; Gutowsky, H. S. *J. Chem. Phys.* **1995**, *87*, 4383.
(26) Gutowsky, H. S.; Arunan, E.; Emilsson, T.; Tschopp, S. L.; Dykstra, C. E. *J. Chem. Phys.* **1995**, *103*, 3917.
(27) Arunan, E.; Emilsson, T.; Gutowsky, H. S.; Dykstra, C. E. *J. Chem. Phys.* **2001**, *114*, 1242.
(28) Xu, Y.; Jäger, W. *J. Chem. Phys.* **1997**, *107*, 4788.
(29) Bunker, P. R.; Jensen, P. *Molecular Symmetry and Spectroscopy*, 2nd ed. NRC Press: Ottawa, 1998.
(30) Townes, C. H.; Schawlow, A. L. *Microwave Spectroscopy*; Dover: New York, 1975.

Table 1. Summary of Molecular Symmetry Group Theory Analysis for the Metastable States of the Ne_3-NH_3 Isotopomers

	Ne_3-NH_3	Ne_3-ND_3	Ne_3-ND_2H	Ne_3-NDH_2
molecular symmetry group	G_{36}	G_{36}	G_{12}	G_{12}
total symmetry required[a]	A_2/A_4	A_1/A_3	A_1'/A_2'	A_1''/A_2''
nuclear spin symmetry[b]	$4A_1\oplus 2E_1$	$10A_1\oplus A_3\oplus 8E_1$	$6A_1'\oplus 3A_1''$	$3A_1'\oplus A_1''$
rotational symmetry				
$K = 0$ (even J/odd J)	A_1/A_3		A_1'/A_2'	
$K = 3n$	$A_1\oplus A_3$		$A_1'\oplus A_2'$	
$K \neq 3n$	E_3		E'	
NH_3 inversion symmetry	symmetric/antisymmetric		symmetric/antisymmetric	
	A_1/A_4		A_1''/A_2''	
NH_3 internal rotation symmetry	ground state/first excited state		ground state/first excited state	
	A_1/E_1		n/a	
	metastable tunneling states		metastable tunneling states	
rovibrational symmetry[c]	$\Sigma 0_{0s}$, $\Sigma 0_{0a}$, $\Sigma 1_{1s}$		$\Sigma 0_{0s}$	$\Sigma 0_{0a}$
$K = 0$ (even J/odd J)	A_1/A_3, A_4/A_2, E_1/E_2		A_1'/A_2'	A_2''/A_1''
$K = 3n$	$A_1\oplus A_3$, $A_4\oplus A_2$, $E_1\oplus E_1$		$A_1'\oplus A_2'$	$A_2''\oplus A_1''$
$K \neq 3n$	E_3, E_4, G		E'	E''
predicted nuclear spin	$\Sigma 0_{0s}$:$\Sigma 0_{0a}$:$\Sigma 1_{1s}$		$\Sigma 0_{0s}$:$\Sigma 0_{0a}$	
statistical weights	0:4:2	10:1:8	6:3	1:3

[a] Refers to the symmetry of the total wave function upon exchange of identical fermions or bosons. [b] Refers to the symmetry of the nuclear spin function of the identical hydrogen or deuterium nuclei only. [c] Includes the NH_3 inversion and NH_3 internal rotation symmetries.

Table 2. Spectroscopic Constants Obtained for Ne_3-NH_3 and $Ne_3-{}^{15}NH_3$

$\Sigma 0_{0a}$	$^{22}Ne_3-NH_3$	$^{20}Ne_3-NH_3$	$^{22}Ne_3-{}^{15}NH_3$	$^{20}Ne_3-{}^{15}NH_3$
		Rotational Constant/MHz		
B	1971.5299(2)	2074.4130(1)	1925.4918(2)	2025.5516(2)
		Centrifugal Distortion Constant/kHz		
D_J	64(1)	71(1)	60(1)	67(1)
		^{14}N Quadrupole Hyperfine Constant/MHz		
χ_{aa}	0.4007(18)	0.3939(12)		
		Standard Deviation/kHz		
σ	2.7	3.2	0.9	1.0

pomers: $^{20}Ne_3-NH_3$, $^{22}Ne_3-NH_3$, $^{20}Ne_3-{}^{15}NH_3$, and $^{22}Ne_3-{}^{15}NH_3$. The four transitions correspond to the $K = 0$ progression of each species, and the transition frequencies are provided as Supporting Information in Tables S1 and S2. From the relative intensities, an effective rotational temperature of about 0.8 K was estimated. The highest J transition measured for each isotopomer corresponds to $J = 4-3$. Only the $K = 0$ components were observed despite a careful search over tens of MHz for the weaker $K = 3$ component, probably because of insufficient intensity. The ^{14}N nuclear quadrupole hyperfine structure was resolved for the two lowest J transitions ($J_K = 1_0-0_0$ and 2_0-1_0) of the $^{20}Ne_3-NH_3$ and $^{22}Ne_3-NH_3$ isotopomers. The ^{14}N hyperfine and rotational analyses were done simultaneously for these two isotopomers using Pickett's global fitting program.[31] For the ^{15}N-containing species, the same program was used for the rotational fit. The resulting spectroscopic constants are compared for each of the four isotopomers in Table 2.

As reported for Ar_3-NH_3,[20] there is a second metastable state, $\Sigma 1_1$, of $^{20}Ne_3-NH_3$ associated with the E_1 nuclear spin function in Table 1. A spectral search was carried out at both higher and lower frequencies than the ground-state transition frequencies, but no transitions were found that could be assigned to the excited internal rotor state based on the expected intensity and ^{14}N hyperfine splitting. The $\Pi 1_1$ states should have a larger dipole moment since the ammonia axis is aligned with the C_3 axis of the cluster. However, these states are not metastable, and no transitions belonging to these states could be assigned.

3.2. $^{20}Ne_3-ND_3$. The molecular symmetry group analysis of $^{20}Ne_3-ND_3$ is similar to that of Ar_3-ND_3[20] and is summarized in Table 1. The spectrum predicted for the ground internal rotor state is similar to that of the $^{20}Ne_3-NH_3$ symmetric rotor with the important distinction that an inversion tunneling splitting is anticipated for the ND_3-containing species. The crucial difference that enables this observable tunneling splitting is a result of the nuclear spin function that characterizes the three bosons (deuterium nuclei) versus that of the three fermions (protons) in the symmetry analysis. The two inversion tunneling components of the ground internal rotor state have predicted spin statistical weights of 10 and 1 for the $\Sigma 0_{0s}$ and $\Sigma 0_{0a}$ states, respectively. The tunneling splitting was anticipated to be very small as reported for the Ar_3-ND_3 tetramer in which the B rotational constants of the two states differed by only 18 kHz.[20]

Four rotational transitions were initially measured and assigned to the more intense $\Sigma 0_{0s}$ state of $^{20}Ne_3-ND_3$. As described for $^{20}Ne_3-NH_3$, these observed transitions are part of the $K = 0$ progression. Transitions corresponding to the weaker $\Sigma 0_{0a}$ state were found at slightly lower frequencies than their symmetric counterparts, but the inversion tunneling splitting was too small to be resolved for the lowest energy transition, $J_K = 1_0-0_0$. In fact, the observed splitting for the 2_0-1_0 transition was only 10 kHz which approaches the resolution limit of the spectrometer ($\sim$7 kHz). The ^{14}N nuclear quadrupole hyperfine splitting was resolved for all four rotational transitions of the symmetric state. For the weaker $\Sigma 0_{0a}$ state, the ^{14}N hyperfine structure was not resolved since the observed spectral lines overlapped too closely with those of the more intense

(31) Pickett, H. M. *J. Mol. Spectrosc.* **1991**, *148*, 371.

Table 3. Spectroscopic Constants for Ne_3-ND_3, Ne_3-ND_2H, and Ne_3-NDH_2

$\Sigma 0_{0s}/\Sigma 0_{00s}$	$^{20}Ne_3$–ND_3	$^{20}Ne_3$–ND_2H	$^{20}Ne_3$–NDH_2
B/MHz	1943.7354(1)	1984.0396(2)	2027.0382(2)
D_J/kHz	57.1(1)	63.1(1)	68.40(1)
χ_{aa}/MHz	0.694(1)	0.639(2)	0.510(1)
F /kHz	3.3	7.5	6.6
$\Sigma 0_{0a}/\Sigma 0_{00a}$	$^{20}Ne_3$–ND_3	$^{20}Ne_3$–ND_2H	$^{20}Ne_3$–NDH_2
B/MHz	1943.7307(1)	1984.1007(2)	2027.2749(2)
D_J/kHz	57.1[a]	63.0(1)	68.4(1)
χ_{aa}/MHz	0.694[a]	0.643(3)	0.501((1)
σ/kHz	4.7	8.5	3.3

[a] Fixed at value from symmetric inversion state.

symmetric tunneling state. Consequently, it was necessary to fix the χ_{aa} constant at the $\Sigma 0_{0s}$ state value in the fit of the $\Sigma 0_{0a}$ state transitions. The ^{14}N hyperfine and rotational fits were done together using Pickett's program[31] for each of the two inversion states, and the spectroscopic constants are given in Table 3. The measured transition frequencies are given in Table S3 (Supporting Information).

A spectral search was carried out for the excited internal rotor state associated with the E_1 nuclear spin function at both higher and lower frequencies than the ground-state transitions. As in the other tetramer species, no transitions were found that matched the intensity and ^{14}N hyperfine patterns expected for the excited state.

3.3. $^{20}Ne_3-ND_2H$. The $^{20}Ne_3-ND_2H$ tetramer follows the molecular symmetry group analysis outlined for Ar_3-ND_2H[20] and is summarized in Table 1. The symmetric top spectrum of the ground internal state of $^{20}Ne_3-ND_2H$ is expected to consist of two inversion tunneling components with relative intensities of 6 and 3 for the $\Sigma 0_{00s}$ and $\Sigma 0_{00a}$ states, respectively. Unlike the NH_3- and ND_3-containing species, there are no metastable internal rotor states of $^{20}Ne_3-ND_2H$ and thus only the ground-state spectrum was sought.

The transition frequencies assigned to the two inversion tunneling components of the ground internal rotor state of $^{20}Ne_3-ND_2H$ are provided as Supporting Information in Table S4. Four $K = 0$ transitions were measured for each state, and the inversion tunneling splitting is approximately 140 kHz for the $J_K = 1_0-0_0$ transition. The ^{14}N nuclear quadrupole hyperfine patterns overlap for the lowest J transition only. The more intense tunneling components appear at a lower frequency and were therefore assigned to the $\Sigma 0_{00s}$ inversion state. This is the opposite of the assignment in the ND_3-containing isotopomer in which the symmetric inversion components were found at higher frequencies. The rotational and ^{14}N hyperfine fits were done for each inversion state as described for $^{20}Ne_3-NH_3$, and the spectroscopic constants are listed in Table 3.

3.4. $^{20}Ne_3-NDH_2$. The molecular symmetry group analysis of $^{20}Ne_3-NDH_2$ tetramer is analogous to that described for Ar_3-NDH_2,[20] and the important symmetry considerations are given in Table 1. The ground internal rotor state spectrum is expected to be split into two due to the inversion of the NDH_2 moiety. The nuclear spin statistical weights are 1 and 3 for the $\Sigma 0_{00s}$ and $\Sigma 0_{00a}$ inversion states, respectively. As with $^{20}Ne_3-ND_2H$, there are no metastable internal rotor states of $^{20}Ne_3-NDH_2$.

Four rotational transitions were measured and assigned to the $K = 0$ progression of the $^{20}Ne_3-NDH_2$ isotopomer. The transition frequencies for the two inversion tunneling states of the are included as Supporting Information in Table S5. The inversion tunneling components are split by 475 kHz for the lowest transition, $J_K = 1_0-0_0$, allowing complete spectral separation of the ^{14}N nuclear quadrupole hyperfine patterns for each transition of the two inversion states. As in the $^{20}Ne_3-ND_2H$ isotopomer, the lower frequency components were assigned to the $\Sigma 0_{00s}$ state based on the predicted intensities. The transitions were fit as described for $^{20}Ne_3-NH_3$ for each of the two inversion states, and the spectroscopic constants are listed in Table 3.

Table 4. Summary of Molecular Symmetry Group Theory Analysis for the Metastable States of the $^{20}Ne_2{}^{22}Ne-NH_3$ and $^{20}Ne^{22}Ne_2-NH_3$ Isotopomers

	$^{20}Ne_2{}^{22}Ne$–NH_3	$^{20}Ne^{22}Ne_2$–NH_3
molecular symmetry group	G_{12}	
total symmetry required[a]	A_2'/A_2''	
nuclear spin symmetry[b]	$4A_1' \oplus 2E'$	
rotational symmetry[c]	K_aK_c = ee/eo/oe/oo	
	$A_1'/A_1''/A_1'/A_1''$	$A_1'/A_1''/A_1''/A_1'$
NH_3 inversion symmetry	symmetric/antisymmetric	
	A_1'/A_2'	
NH_3 internal rotation symmetry	ground state/first excited state	
	A_1'/E'	
rovibrational symmetry[d]	K_aK_c = ee/eo/oe/oo	
$\Sigma 0_{0s}$	$A_1'/A_1''/A_1'/A_1''$	$A_1'/A_1''/A_1''/A_1'$
$\Sigma 0_{0a}$	$A_2'/A_2''/A_2'/A_2''$	$A_2'/A_2''/A_2''/A_2'$
$\Sigma 1_{1s}$	$E'/E''/E'/E''$	$E'/E''/E''/E'$
predicted nuclear spin	$\Sigma 0_{0s}:\Sigma 0_{0a}:\Sigma 1_{1s}$	
statistical weights	0:4:2	10:1:8

[a] Refers to the symmetry of the total wave function upon exchange of identical fermions or bosons. [b] Refers to the symmetry of the nuclear spin function of the identical hydrogen or deuterium nuclei only. [c] Depends on whether K_a and K_c are even (e) or odd (o). [d] Includes the NH_3 inversion and NH_3 internal rotation symmetries.

3.5. $^{20}Ne_2{}^{22}Ne-NH_3$ and $^{20}Ne_2{}^{22}Ne-{}^{15}NH_3$. The molecular symmetry analysis of the asymmetric tops, $^{20}Ne_2{}^{22}Ne-NH_3$ and $^{20}Ne_2{}^{22}Ne-{}^{15}NH_3$, is described in more detail here since it is unique in comparison to the previously studied Rg_3-NH_3 complexes. A summary of the symmetry details is found in Table 4. The three identical hydrogen nuclei and two ^{20}Ne nuclei in $^{20}Ne_2{}^{22}Ne-NH_3$ can be permuted to create 24 distinct versions of the complex. The complete nuclear permutation inversion group is then G_{24} and can be reduced to G_{12} if the tunneling motion that reverses the handedness of the Ne_3 ring is neglected. The total wave function symmetry must be A_2' or A_2'' since it must be symmetric with respect to the exchange of the identical bosons (^{20}Ne atoms) and antisymmetric with respect to the interchange of any two identical fermions (hydrogen atoms). The hydrogen nuclear spin function is of $4A_1' \oplus 2E_1'$ symmetry. For the ground internal rotor state, $\Sigma 0_0$, the rovibrational symmetry alternates A_1'/A_1'' for even/odd values of K_c for the symmetric inversion component and A_2'/A_2'' for the antisymmetric inversion component. The rotational energy levels of the $\Sigma 0_{0s}$ state of $^{20}Ne_2{}^{22}Ne-NH_3$ have a nuclear spin statistical weight of zero since the nuclear spin function does not contain a suitable symmetry to achieve the required total wave function symmetry. Thus, no rotational transitions are observable for the symmetric state. For the $\Sigma 0_{0a}$ state, all of the rotational levels can combine with the A_1' nuclear spin symmetry to give either A_2' or A_2'' total symmetry and, therefore, all rotational levels in this state have a nonzero spin statistical weight. Due to the orientation of the complex in its principal inertial axis system (Figure 1b), *a*- and *b*-type transitions were expected between these energy levels.

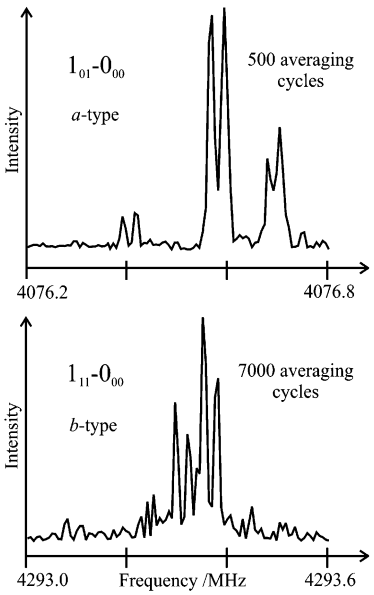

Figure 2. Spectra comparing the relative intensities of *a*-type (upper trace) and *b*-type (lower trace) transitions observed for $^{20}Ne_2{}^{22}Ne-NH_3$. The ^{14}N hyperfine splitting was fit to obtain $\chi_{aa} = 0.393(7)$ MHz and $\chi_{bb} = -0.141(11)$ MHz.

In total, 17 rotational transitions were measured for the $\Sigma 0_{0a}$ state of $^{20}Ne_2{}^{22}Ne-NH_3$, and the transition frequencies are included with the Supporting Information in Table S6. These include 14 *a*-type transitions and three *b*-type transitions. The *b*-type transitions were observed to be much weaker than the *a*-type transitions due to the smaller dipole moment component along the *b*-axis of the tetramer as shown from the geometry in Figure 1b. A comparison of the observed intensities of the lowest energy *a*-type ($J_{K_aK_c} = 1_{01}-0_{00}$) and *b*-type ($1_{11}-0_{00}$) transitions is shown in Figure 2. The ^{14}N nuclear quadrupole hyperfine structure was initially fit using a first-order program, and the resulting χ_{aa} and χ_{bb} constants were held fixed during the subsequent rotational fit. The rotational fit was done in Pickett's program using Watson's I^r S-reduction Hamiltonian[31] to obtain rotational constants *A*, *B*, and *C* and quartic centrifugal distortion constants D_J, D_{JK}, D_K, d_1, and d_2. The A rotational constant and D_K centrifugal distortion constant were highly correlated in the preliminary fit, and as a result, the value of D_K was set to zero in the final analysis. The spectroscopic constants determined for $^{20}Ne_2{}^{22}Ne-NH_3$ are listed in Table 5.

The corresponding 17 rotational transitions were measured and assigned for the $^{20}Ne_2{}^{22}Ne-{}^{15}NH_3$ isotopomer, and the frequencies are provided in the Supporting Information Table S7. The rotational fit was analogous to that described above for the NH_3-containing species, and the resulting spectroscopic constants are given in Table 5 with those of $^{20}Ne_2{}^{22}Ne-NH_3$.

3.6. $^{20}Ne^{22}Ne_2-NH_3$ and $^{20}Ne^{22}Ne_2$-$^{15}NH_3$. The G_{12} character table was also used in the molecular symmetry group analysis of the $^{20}Ne^{22}Ne_2-NH_3$ isotopomer using the same procedure described for $^{20}Ne_2{}^{22}Ne-NH_3$. The results are summarized in Table 4. Due to the different orientation in the principal inertial axis system in comparison to the $^{20}Ne_2{}^{22}Ne-NH_3$ isotopomer (Figure 1b and c), the rotational symmetries alternate A_1'/A_1'' for even/odd values of K_b for $^{20}Ne^{22}Ne_2-NH_3$. The asymmetric rotor energy levels (K_aK_c) therefore have the following rovibrational symmetries: A_1' (ee, oo)/A_1'' (eo, oe) for the symmetric inversion component and A_2' (ee, oo)/A_2'' (eo, oe) for the antisymmetric inversion component of the ground internal rotor state. For the $\Sigma 0_{0s}$ state of $^{20}Ne^{22}Ne_2-NH_3$, no rotational transitions are observable as the energy levels have nuclear spin statistical weights of zero. Conversely, all rotational levels in the $\Sigma 0_{0a}$ state have nonzero spin statistical weights, and *a*- and *c*-type transitions were expected since there is a nonzero dipole moment contribution along the *a*- and *c*-axes as demonstrated in Figure 1c.

Sixteen rotational transitions were measured and assigned to the $\Sigma 0_{0a}$ state of the $^{20}Ne^{22}Ne_2-NH_3$ complex, including 14 *a*-type and two *c*-type transitions. The transition frequencies are provided as Supporting Information in Table S8. The *c*-type transitions are extremely weak and could only be observed after several thousand averaging cycles. This is due to a combination of the small dipole moment component along the *c*-axis of the complex and the low abundance of the $^{20}Ne^{22}Ne_2-NH_3$ species in the molecular beam expansion. The spectroscopic constants were determined following the procedure described for the $^{20}Ne_2{}^{22}Ne-NH_3$ isotopomer and are listed in Table 5.

The corresponding rotational transitions for the $^{20}Ne_2{}^{22}Ne-{}^{15}NH_3$ isotopomer are given in the Supporting Information Table S9. The rotational fit was analogous to that described above for the $^{20}Ne^{22}Ne_2-NH_3$-containing species, and the spectroscopic constants are listed in Table 5 with those of the other asymmetric top isotopomers.

4. Ab Initio calculations for Ne_3-NH_3

Ab initio calculations were done at the CCSD(T) level of theory using the MOLPRO software package.[32] Three separate potential energy surfaces were constructed for the Ne_3-NH_3 tetramer which correspond to three NH_3 umbrella angles: $\angle HNH = 106.67°$, $\angle HNH = 113.34°$, and $\angle HNH = 120.00°$. The N−H bond length was held fixed at the experimental value of 1.012 42 Å.[33] The interaction energy of the tetramer was calculated via the supermolecular approach.[34] Preliminary calculations were attempted using Sadlej's VTZ (N, H)[35] and Dunning's aug-cc-pVTZ (Ne)[36] bases augmented with (3s, 3p, 2d) bond functions along each van der Waals bond as done earlier for the $Ne-NH_3$ dimer[16] and Ne_2-NH_3 trimer.[18] These calculations did not run to completion due to scratch file size limitations. As a result, the ab initio calculations for the Ne_3-NH_3 tetramer had to be done using a smaller Ne basis set, Dunning's aug-cc-pVDZ.[36] To allow comparison with the previously published potential energy surfaces of the dimer and trimer complexes, it was necessary to recalculate select regions of the $Ne-NH_3$ dimer and Ne_2-NH_3 trimer potential energy surfaces using this smaller Ne basis set.

The interaction energy was determined as a function of θ, ϕ, and *R* (Figure 3) for each of the three NH_3 monomer geometries. To reduce the dimension of the calculations, the C_3 axis of NH_3 was constrained to lie in the *ac*-plane. This particular position of the C_3 axis was chosen since the NH_3 substituent is then symmetrically oriented about the *ac*-plane for all θ values when

(32) Werner, H. J.; Knowles, P. R. (with contributions from Amos, R. D.; Bernhardsson, A.; Berning, A.; Celani, P.; Cooper, D. L.; McNicholas, M. J. O.; Manby, F. R.; Meyer, W.; Mura, M. E.; Nicklass, A.; Palmieri, P.; Pitzer, R.; Rauhut, G.; Schütz, M.; Stoll, H.; Stone, A. J.; Tarroni, R.; Thorsteinsson, T.) *MOLPRO*, version 2000.1; University of Birmingham: U.K., 1999.
(33) Benedict W. S.; Plyler, E. K. *Can. J. Phys.* **1957**, *35*, 1235.
(34) Boys S. F.; Bernardi, F. *Mol. Phys.* **1970**, *19*, 553.
(35) Sadlej, A. J. *Collect. Czech. Chem. Commun.* **1988**, *53* 1995.
(36) Dunning, T. H., Jr. *J. Chem. Phys.* **1989**, *90*, 1007.

Table 5. Spectroscopic Constants for $^{20}Ne_2{}^{22}Ne-NH_3$ and $^{20}Ne^{22}Ne_2-NH_3$

$\Sigma 0_{0a}$	$^{20}Ne_2{}^{22}Ne-NH_3$	$^{20}Ne_2{}^{22}Ne-{}^{15}NH_3$	$^{20}Ne^{22}Ne_2-NH_3$	$^{20}Ne^{22}Ne_2-{}^{15}NH_3$
		Rotational Constants/MHz		
A	2281.1446(6)	2280.9266(8)	2213.8723(8)	2213.8077(7)
B	2064.2307(3)	2015.4579(4)	2032.7092(3)	1984.4307(2)
C	2012.6450(3)	1965.9071(3)	1976.2194(3)	1930.7222(2)
		Centrifugal Distortion Constants/kHz		
D_J	69.6(1)	64.8(1)	66.9(1)	62.3(1)
D_{JK}	80.9(1)	84.9(1)	76.0(1)	79.6(1)
d_1	−2.22(1)	−1.96(1)	−1.76(1)	−1.50(1)
d_2	−1.22(1)	−1.02(1)	1.32(1)	1.02(1)
		^{14}N Quadrupole Hyperfine Constants/MHz		
χ_{aa}	0.393(7)		0.389(5)	
χ_{bb}	−0.141(11)		−0.113(8)	
		Standard Deviation/kHz		
σ/kHz	17.4	5.1	10	7.8

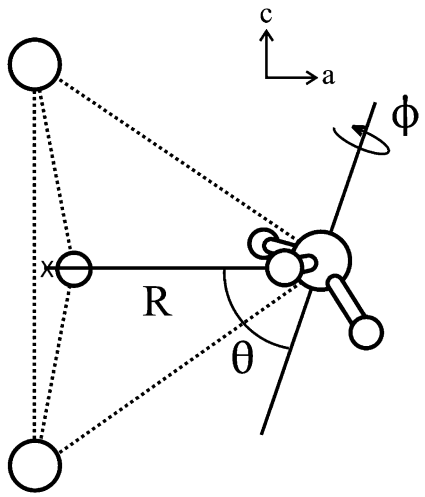

Figure 3. Coordinate system of Ne_3-NH_3 for the ab initio calculations. R is the distance between the center of mass of the Ne_3 ring and the nitrogen atom. All of the calculations were to done by restricting the C_3 axis of NH_3 orientations lying in the *ac*-plane. The angle θ denotes the angle between the C_3 axis of NH_3 and R. When $= \theta$ is 0°, the C_3 axis of NH_3 aligned with R and the hydrogen atoms point toward the Ne_3 ring. The angle ϕ describes the orientation of NH_3 upon rotation about its C_3 axis. When $\theta = 90°$, $\phi = 0°$ corresponds to the orientation in which the C_3 axis of NH_3 is perpendicular to R and one hydrogen atom is pointed toward the Ne_3 ring. When $\theta = 90°$ and $\phi = 60°$, two hydrogen atoms point toward the Ne_3 ring.

$\phi = 0°$ or $\phi = 60°$. This allows the investigation of the NH_3 inversion motion in a symmetric environment when the C_3 axis of NH_3 is perpendicular to *R*. The Ne−Ne van der Waals bond length[28] was fixed at 3.29 Å as done previously for Ne_2-NH_3 to further reduce the degrees of freedom to a computationally manageable level. The angle θ was varied between 0° and 180° in increments of 30° for two different values of ϕ, 0°, and 60°. For each value of θ, the distance *R* was varied in steps of 0.1 Å until the minimum energy was located. Steps of 0.05 Å were then taken to each side of this minimum to reduce the uncertainty in the radial coordinate. An additional angle, $\theta = 105°$, was included to further narrow the position of the potential energy surface minimum. Ab initio results for the Ne_3-NH_3 complex are summarized in the Supporting Information Tables S10−S12 for the three NH_3 monomer geometries.

5. Discussion

The following discussion is divided into four parts. The first deals with the analysis of the ^{14}N nuclear quadrupole hyperfine structures and the large amplitude internal rotation of NH_3 within the Ne_3-NH_3 tetramer. The van der Waals bond distances are estimated from the rotational constants in the second section, followed by a discussion of the observed inversion tunneling splittings of the deuterated isotopomers. The final section deals with the ab initio potential energy surfaces and relates the determined topological features to experimental observations of Ne_3-NH_3. In all four sections, comparisons are made with earlier studies of the related Rg_n-NH_3 systems so as to provide the reader with a summary of the entire cluster family.

5.1. ^{14}N Nuclear Quadrupole Hyperfine Structures. The observed microwave spectra of the $^{20}Ne_3-NH_3$ and $^{22}Ne_3-NH_3$ tetramers are consistent with the initial prediction that these are symmetric top molecules as reported earlier for Ar_3-NH_3.[20] In the Ar-containing tetramer, transitions in the $K = 0$, 3, and 6 progressions were observed. The absence of other transitions suggests a structure in which the three Ar atoms are symmetrically arranged in a triangle about the C_3 axis of the tetramer and that the NH_3 subunit undergoes sufficiently large amplitude motions that its molecular dipole moment does not contribute to the observed rotational spectrum. This latter assertion is strongly supported by the small ^{14}N quadrupole coupling constants of Ar_3-NH_3 (χ_{cc}= 0.1458 MHz) and holds also for Ne_3-NH_3. The rotational transitions are mainly driven by the small dipole moment induced by the interactions between the rare gas atoms and ammonia. For the Ne_3-NH_3 symmetric tops reported in this work, only the $K = 0$ transitions were measured; the highest *J* transition being $J = 4-3$. Since the $^{20}Ne_3$- and $^{22}Ne_3$-containing complexes are expected to be prolate symmetric tops, the $K = 3$ progression is higher in energy than the $K = 0$ progression[30] and the energy levels were presumably too sparsely populated in the molecular beam expansion for the $K = 3$ transitions to be measured. This thermal relaxation argument is further supported by the fact that higher *J* transitions were within the range of the spectrometer but could not be observed.

The presence of ^{14}N nuclear quadrupole hyperfine structures helped with the assignment of rotational transitions, particularly for the two asymmetric tops, $^{20}Ne_2{}^{22}Ne-NH_3$ and $^{20}Ne^{22}Ne_2-NH_3$. Since the spectra of the various isotopomers of Ne_3-NH_3 support a model in which the NH_3 undergoes large amplitude internal motions, the ^{14}N nuclear quadrupole coupling constants should be viewed as highly averaged over these motions. Following the analysis of the previously studied Rg_n-NH_3

Table 6. Estimated Orientation of Ammonia in the Ar_3-NH_3 and Ne_3-NH_3 Complexes

	$\Sigma 0_{0a}/\Sigma 0_{00a}$	$-NH_3$	$-NDH_2$	$-ND_2H$	$-ND_3$
		tetramers			
Ar_3[a]	θ	56.2°/123.8°	56.9°/123.1°	57.6°/122.4°	58.0°/122.0°
	$\langle P_2(\cos q)\rangle$	−0.036	−0.053	−0.070	−0.079
$^{20}Ne_3$	θ	58.8°/121.2°	60.2°/120.0°	61.4°/118.6°	62.0°/118.0°
	$\langle P_2(\cos q)\rangle$	−0.096	−0.125	−0.156	−0.170
		trimers			
Ar_2[b]	$\langle P_2(\cos q)\rangle$	−0.190	−0.211	−0.230	−0.253
$^{20}Ne_2$[c]	$\langle P_2(\cos q)\rangle$	−0.082	−0.107	−0.129	−0.156
		dimers			
Kr[d]	$\langle P_2(\cos q)\rangle$	−0.061	−0.085	−0.104	−0.126
Ar[e]	$\langle P_2(\cos q)\rangle$	−0.086	−0.115	−0.141	−0.166
Ne[f]	$\langle P_2(\cos q)\rangle$	−0.066	−0.086	−0.105	−0.128

[a] Reference 20. [b] Reference 19. [c] Reference 18. [d] Reference 17. [e] References 11 and 14. [f] Reference 16.

complexes, the following equation defines the relationship between ^{14}N nuclear quadrupole coupling constant and the orientation and dynamics of the NH_3 subunit in Ne_3-NH_3: $\chi_{aa} = {}^1/_2\chi_o(NH_3)\langle 3\cos^2\theta - 1\rangle$, where χ_o is the quadrupole coupling constant of free NH_3 (− 4.0898 MHz),[37] θ is the angle between the C_3 axis of NH_3 and the C_3 axis of the tetramer, and the brackets indicate averaging over the large amplitude motions of the tetramer. The Legendre factor, $\langle P_2(\cos\theta)\rangle = \langle 3\cos^2\theta - 1\rangle$, is zero in the limit of free internal rotation of NH_3, and thus, for sufficiently large amplitude internal motions, the above equation cannot be used to easily extract accurate information about the orientation of NH_3 within the complexes. With this in mind, the results for θ and $\langle P_2(\cos\theta)\rangle$ are given in Table 6 for the symmetric top isotopomers of $^{20}Ne_3$. As seen in the other Rg_n-NH_3 complexes, the Legendre factor increases for the heavier, deuterated isotopomers due to the larger tunneling masses and lower zero point energies. The Legendre factors of the $Rg-NH_3$, Rg_2-NH_3, and Ar_3-NH_3 complexes are included in Table 6 for easy comparison. Surprisingly, the values for the Ar_3-containing isotopomers are smaller than those for the Ne_3-containing isotopomers. This is the reverse of the trend observed in the dimers and trimers for which the Ne analogues have smaller $\langle P_2(\cos\theta)\rangle$ values as expected since Ne is less polarizable and expected to form weaker van der Waals bonds by comparison. In the Ne-containing clusters, the Legendre factors increase in moving from the dimer to the trimer and then again to the tetramer suggesting that the internal rotation of NH_3 in the θ coordinate becomes successively more hindered when solvated by additional Ne atoms. The same effect occurs between the $Ar-NH_3$ dimer and Ar_2-NH_3 trimer, but the Ar_3-NH_3 tetramer has a surprisingly small $P_2\langle\cos\theta\rangle$ value by comparison. This suggests that the barrier to internal rotation of NH_3 in the θ coordinate is comparatively lower in the Ar_3-NH_3 complex. In a physical sense, the NH_3 molecule experiences a more isotropic environment when bound to three Ar atoms instead of one or two. This is supported by the infrared study by Abouaf−Marguin et al.[38] in which the authors found that NH_3 undergoes nearly free internal rotation when enclosed in solid Rg matrixes. The contradictory observations for the Ar- and Ne-containing tetramers indicate that the internal motions of NH_3 are still critically influenced by the size and polarizability of the individual Rg atoms in these microscopic clusters. Such fundamental anomalies will be reflected in the potential energy surfaces of the two quaternary complexes. With the addition of more Ne atoms, it is expected that the ^{14}N nuclear quadrupole coupling constants will eventually decrease as observed for Ar_3-NH_3 since the internal rotor dynamics of NH_3 solvated with Ne are similar to those with Ar as the bulk limit (matrix) is approached.

Table 7. Comparison of Bond Lengths (Å) for various van der Waals Dimers, Trimers, and Tetramers

	R(Ne–X)	r(Ne–Ne)		R(Ar–X)	r(Ar–Ar)
Ne_3-NH_3	3.681	3.388	Ar_3-NH_3[c]	3.814	3.866
Ne_2-NH_3[a]	3.695	3.26	Ar_2-NH_3[d]	3.835	3.818
$Ne-NH_3$[b]	3.723	n/a	$Ar-NH_3$[e]	3.8359	n/a
Ne_3-Ar[f]	3.601	3.28	Ar_3-Ne[f]	3.61	3.826
Ne_2-Ar[f]	3.605	3.282	Ar_2-Ne[f]	3.595	3.818
$Ne-Ar$[g]	3.607	n/a	$Ar-Ne$[g]	3.607	n/a

[a] Reference 18. [b] Reference16. [c] Reference 20. [d] Reference 19. [e] Reference 11. [f] Reference 28. [g] Reference 39.

5.2. van der Waals Bond Lengths. Estimates of van der Waals bond lengths in weakly bound complexes can be made using standard moment of inertia expressions. For weakly bound trimers and tetramers, there are often small deviations in the experimentally determined bond lengths when compared with the known dimer bond distances, and this provides an indication of the importance of nonadditive contributions to the interaction energies of such clusters. For the symmetric top Ne_3-NH_3 complexes, there is only one rotational constant available to estimate the structure, and this constant should be regarded as being highly averaged over the large zero point vibrational motions of the weakly bound complex. Assuming a spherical geometry of the internal rotational wave function of the ammonia moiety in the ground state of NH_3 (as supported by the small χ_{aa} values), a rough approximation of the Ne−Ne and $Ne-NH_3$ bond lengths can be made using the following expression for a symmetric top molecule:[30]

$$I_B = m_{Ne}d^2(1-\cos\alpha) + m_{Ne}m_{NH_3}d^2(1+2\cos\alpha)/(3m_{Ne}+m_{NH_3})$$

where d is the distance from the Ne atom to the center of mass of NH_3 and a is the Ne−(NH_3)−Ne angle. Using the B rotational constants for the $^{20}Ne_3-NH_3$ and $^{20}Ne_3-{}^{15}NH_3$ isotopomers, a set of two equations is formed which can be solved for d and α. The Ne−Ne bond length can be determined trigonometrically, and the results are given in Table 7 for Ne_3-NH_3 along with the corresponding van der Waals bond lengths of the $Ne-NH_3$ dimer and Ne_2-NH_3 trimer. The analogous values for the Ar_n-NH_3 cluster series are also included in Table 7. For both the Ar- and Ne-containing complexes, the $Rg-NH_3$ bond decreases in length as the size of the cluster increases. The decrease is on the order of 0.014 Å for the Ne-containing species between the dimer and tetramer complexes and 0.022 Å in the corresponding Ar species. Another trend is the lengthening of the Rg−Rg bond in the Rg_3-NH_3 tetramers relative to the Rg_2-NH_3 trimers. The Ne−Ne bond lengthens by 0.128 Å, and the Ar−Ar bond lengthens by 0.048 Å. Similar trends are observed in the van der Waals bond lengths of the Ar_n-Ne and Ne_n-Ar complexes[28,39] which are provided in Table 7 for comparison. These small variations in the van der Waals bond lengths as a function

(37) Marshall, M. D.; Muenter, J. S. *J. Mol. Spectrosc*. **1981**, *85*, 322.
(38) Abouaf-Marguin, L.; Jacox, M. E.; Milligan, D. E.; *J. Mol. Spectrosc*. **1977**, *67*, 24.

of the Rg cluster size indicate that the nonadditive contributions to the interaction energies of these systems are not negligible. These spectroscopic studies thus play a crucial role in extending the understanding of nonadditive contributions by providing empirical information which is necessary for the development and testing of complete and accurate models of weak interactions. Since the monomeric properties of the solvating Rg atom have a fundamental influence on the size of these nonadditive effects, as demonstrated in this work, it is critical to have detailed spectroscopic information for molecules that are microsolvated by different Rg atoms.

5.3. Inversion Tunneling. Ammonia is an attractive candidate for studies of weakly bound complexes from a spectroscopic standpoint since its inversion motion allows a study of the effect of the Rg cluster environment on a soft intramolecular mode. In this work, rotational transitions within the two inversion states were observed for deuterated isotopomers of Ne_3-NH_3 and appeared as small inversion tunneling doublets in the microwave spectra. The differences in the *B* rotational constants, $[B_{\text{antisymmetric}} - B_{\text{symmetric}}]$, of the two inversion states of the $^{20}Ne_3-ND_3$, $^{20}Ne_3-ND_2H$, and $^{20}Ne_3-NDH_2$ isotopomers are −4.7 kHz, 61.1 kHz, and 236.7 kHz, respectively. These small differences in rotational constants indicate that the two inversion states lie close in energy for these three species since, in general, the closer in energy two states are, the more similar their rotational constants. This is further substantiated by the similarity in the observed ^{14}N nuclear quadrupole coupling constants. These differ by only a few kilohertz for the two inversion components of the $^{20}Ne_3-ND_2H$ and $^{20}Ne_3-NDH_2$ complexes.

The inversion tunneling splittings (i.e., twice the difference in *B* rotational constants) in the deuterated Ne_3-NH_3 containing tetramers increase with successive hydrogen substitution as reported previously for the dimer, trimer, and Ar_3-NH_3 tetramer complexes. This is consistent with the trend observed for the energy differences between the symmetric and antisymmetric states of the free ND_3, ND_2H, and NDH_2 monomers that these rotational constants correspond to: 1.6, 5, and 12 GHz, respectively.[40] In Ne_3-ND_3, the symmetric inversion tunneling component is found at higher frequency than the antisymmetric component. The same phenomenon was observed in $Ar-ND_3$,[14] $Kr-ND_3$,[17] Ar_2-ND_3,[19] and Ar_3-ND_3[20] and is the reverse of the assignment in all of the other isotopomers studied. These subtle deviations are a reflection of the sensitive relationship between the intermolecular potential energy surface of each weakly bound cluster and the complicated internal dynamics of the NH_3 subunit. Even for a given potential energy surface of a particular Rg_n-NH_3 complex, the bound state energy levels vary depending on the NH_3 isotopomer. This leads to marked differences in the dynamics of each system depending on the degree of the mixing of internal rotor states and the tunneling probabilities. These variations are apparent in the rotational spectrum of each species. Although a complete understanding of the inversion dynamics of NH_3 cannot be extracted from the rotational spectra alone, Fourier transform microwave spectroscopy provides information that is essential for the construction of accurate empirical potentials that include this motion. This is because the high resolution of the technique allows the measurement of the extremely small inversion tunneling splittings that are characteristic of the deuterated Rg_n-NH_3 complexes.

Table 8. Comparison of Inversion Tunneling Splittings (kHz) for the $Rg-NH_3$, Rg_2-NH_3, and Rg_3-NH_3 Complexes

	$-ND_3$	$-ND_2H$	$-NDH_2$	reference
$^{20}Ne_3$[a]	−9.4	122.2	473.4	this work
$^{20}Ne_2$[b]	19.9	298.1	906.2	18
Ne[a]	55	407.6	1082.2	16
Ar_3[a]	−36	21.4	200.4	20
Ar_2[c]	−165.1	36.1	712	19
Ar[a]	−63	271.6	1101	14
Kr[a]	−85.6	208.4	1038.4	17

[a] $2(B_{\text{antisymmetric}} - B_{\text{symmetric}})$. [b] $(B + C)_{\text{antisymmetric}} - (B + C)_{\text{symmetric}}$. [c] $(A + C)_{\text{antisymmetric}} - (A + C)_{\text{symmetric}}$.

The inversion tunneling splittings observed for the Ne_3-containing tetramers are compared with those of the deuterated isotopomers of the $Rg-NH_3$, Rg_2-NH_3, and Ar_3-NH_3 complexes in Table 8. With the exception of Ar_3-ND_3, the inversion tunneling splittings decrease as additional Rg atoms are added to the cluster. This appears to indicate that the NH_3 inversion motion becomes more hindered in the larger clusters. This observation can be misleading however since the masses of the clusters must also be considered when comparing the differences in the rotational constants. Furthermore, it must be stressed that the observed inversion tunneling splittings are only secondary indications of the energy differences between the $\Sigma 0_{0s}$ and $\Sigma 0_{0a}$ states and not direct measures of the energy splittings between the states. Rotational transitions connecting the $\Sigma 0_{0s}$ and $\Sigma 0_{0a}$ states of the ground internal rotor state are nuclear spin forbidden. Nevertheless, the observation of both inversion components is revealing in itself since it confirms that the NH_3 inversion motion is not quenched when bound to three Rg atoms. This provides some clues to the orientation of NH_3 within the tetramer complex. The observed tunneling splitting suggests that the C_3 axis of NH_3 lies, on average, perpendicular to the C_3 axis of the Rg_3 ring since the inversion motion would be quenched if the environment along the inversion coordinate was asymmetric.[12] In fact, from an infrared study of NH_3 and its deuterated isotopomers embedded in solid Rg matrixes, the inversion barrier was predicted to increase by only 10% in comparison to the free monomer.[38]

5.4. Ab Initio Potential Energy Surfaces. In total, three potential energy surfaces were constructed for the Ne_3-NH_3 van der Waals tetramer corresponding to three different umbrella angles of the NH_3 subunit at the CCSD(T) level of theory. The potential energy surface minimum is $-225.4\ cm^{-1}$ for the experimental equilibrium geometry of NH_3 ($\angle HNH = 106.67°$). The structural coordinates at this minimum energy are $R = 2.95$ Å, $\theta = 105°$, and $\phi = 0°$, corresponding to a tetramer structure in which the C_3 axis of NH_3 is nearly parallel to the plane containing the three Ne atoms (Figure 3). This corresponds to an $Ne-NH_3$ bond length of 3.51 Å in the tetramer complex. This is the same bond length calculated for the Ne_2-NH_3 trimer[18] and is slightly shorter than that estimated from the experimental *B* rotational constant of the Ne_3-NH_3 tetramer (3.68 Å). The ϕ orientation of NH_3 at the potential energy surface minimum is such that one hydrogen atom is pointed toward the Ne_3 ring. The same relative orientation of NH_3 was found for the two surfaces corresponding to the other umbrella angles of NH_3 with minima of $-220.4\ cm^{-1}$ ($\angle HNH = 113.34°$)

(39) Grabow, J.-U.; Pine, A. S.; Fraser, G. T.; Lovas, F. J.; Emilsson, T.; Arunan, E.; Gutowsky, H. S. *J. Chem. Phys.* **1995**, *102*, 1181.
(40) Weiss, M. T.; Strandberg, M. W. P. *Phys. Rev.* **1981**, *83*, 322.

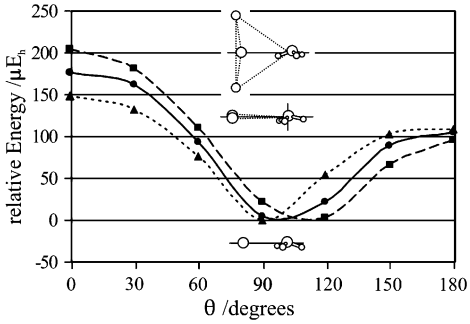

Figure 4. Comparison of the minimum energy dimer [CCSD(T)] paths of the Ne−NH_3 dimer (--▲--), the Ne_2−NH_3 trimer (−●−), and the Ne_3−NH_3 tetramer (− −■− −) as a function of the θ coordinate for ∠HNH = 106.67°. The dimer and trimer minimum energy paths correspond to the ϕ = 60° orientation while the tetramer path corresponds to ϕ = 0°. The global minimum of each curve was set to 0.0 μE_h, and the other energies along the minimum energy paths were adjusted accordingly.

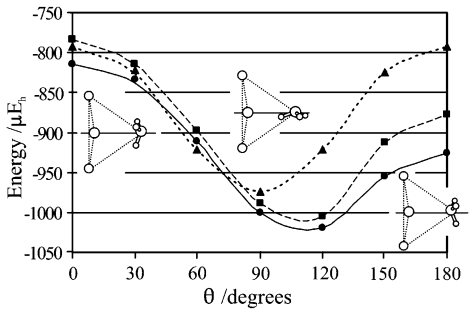

Figure 5. Comparison of the minimum energy as a function of the [CCSD-(T)] paths of Ne_3−NH_3 as a function of the θ coordinate for ϕ = 0° with the C_3 axis of NH_3 lying in the *ac*-plane of the tetramer. Each curve represents a different umbrella angle of ∠NH_3: ∠HNH = 106.67° (−●−), ∠HNH = 113.34° (− −■− −), and ∠HNH = 120.00° (--▲--).

and −213.8 cm^{-1} (∠HNH = 120.00°) at R = 3.05 Å. For internal rotation in the θ coordinate, there are barriers at θ = 0° and θ = 180° for the two nonplanar geometries of NH_3. The barriers are 46.6 cm^{-1}/22.3 cm^{-1}(0°/180°) and 48.6 cm^{-1}/27.9 cm^{-1} for the ∠HNH = 106.67° and ∠HNH = 113.34° NH_3 geometries, respectively. For the planar geometry of NH_3, the barrier is 39.8 cm^{-1} through θ = 0° and θ = 180° due to symmetry.

The topologies of the Ne_3−NH_3 potential energy surfaces can be compared with those of the Ne−NH_3 dimer and Ne_2−NH_3 trimer calculated at the CCSD(T) level of theory using the aug-cc-pVDZ basis set for Ne. The minimum energies for the dimer and trimer complexes using this basis are −60.1 cm^{-1} and −127.9 cm^{-1}, respectively, for the equilibrium NH_3 monomer geometry. The minimum energy paths from θ = 0° to θ = 180° are compared for the Ne−NH_3, Ne_2−NH_3, and Ne_3−NH_3 complexes in Figure 4, and the structures near the potential minima are shown for each cluster. The C_3 axis of NH_3 is nearly perpendicular to the axis joining the nitrogen atom and the center of mass of the Ne_n (n = 1, 2, 3) moiety. For the Ne_3−NH_3 tetramer, the NH_3 subunit is rotated by 60° about its C_3 axis (ϕ = 0°) relative to the dimer and trimer to minimize the repulsion between the hydrogen atoms and the Ne_3 ring. For rotation through the ϕ = 60° orientation of the tetramer, the barrier is 14 cm^{-1} for the potential energy surface corresponding to ∠HNH = 106.67°. The barrier for internal rotation of NH_3 through θ = 0° increases as more Ne atoms are added to the complex. For example, the barriers in the dimer, trimer, and tetramer are 32.5, 38.6, and 45.0 cm^{-1}, respectively, for the equilibrium NH_3 monomer geometry. For rotation through θ = 180°, the barriers are similar in each cluster: 23.8, 22.5, and 20.7 cm^{-1} for Ne−NH_3, Ne_2−NH_3, and Ne_3−NH_3, respectively. The minimum energy path requires 0.4 Å of radial variation in the tetramer, 0.3 Å in the trimer, and 0.5 Å in the dimer. A comparison of the anisotropies of the potential energy curves as a function of the θ coordinate (Figure 4) demonstrates that the angular dependency of the NH_3 orientation is unique in each of the complexes. The potential well becomes broader and deeper with the addition of Ne atoms and the minimum shifts to larger θ values. This corresponds to structures in which the C_3 axis of NH_3 is tilted so that the hydrogen atoms are farther away from the Ne atoms. The broadening of the potential well as successive Ne atoms are added leads to lower zero point energies for the larger clusters. As a result, the tunneling probability decreases as the size of the van der Waals cluster increases. This effect, combined with the larger barriers to internal rotation through θ = 0° for the trimer and tetramer complexes, suggests that motion in the θ coordinate becomes comparatively more hindered with successive Ne atom solvation. This is experimentally supported by the determination of increasing χ_{aa} values in moving from Ne−NH_3[16] to Ne_2−NH_3[18] to Ne_3−NH_3.

The minimum energy paths calculated for the Ne_3−NH_3 tetramer from θ = 0° to θ = 180° are compared for the three different NH_3 internal geometries in Figure 5. As reported previously for the dimer and trimer complexes, the interaction energies are the most similar between θ = 60° and θ = 90°. This indicates that the internal geometry of NH_3 has little influence at these orientations and is in accord with the experimental observation that the NH_3 inversion is barely affected upon complexation if the motion occurs along a symmetric coordinate.[12] Thus, the experimental observation of two inversion tunneling components in the microwave spectra of the deuterated isotopomers of Ne_3−NH_3 is consistent with the assignment to a Σ state, such as the ground internal rotor state of the tetramer complexes. The largest discrepancies between the minimum energy paths are at θ values approaching 180° when the C_3 axis of NH_3 is nearly aligned with the symmetry axis of the tetramer and the hydrogen atoms are pointed away from the Ne_3 ring. This orientation of NH_3 corresponds to a Π internal rotor state of the complex, and the inversion tunneling motion is expected to be quenched for such a geometry.

6. Concluding Remarks

Microwave rotational spectra of 11 isotopomers of $^{20}Ne_3$−NH_3 have been reported for the first time. The spectra, complemented by ab initio potential energy surfaces, complete a study of the prototypical Rg_n−NH_3 cluster series (Rg = Ne, Ar; n = 1−3). Analysis of the rotational constants reveals the importance of nonadditive effects in the Ne_3−NH_3 complexes, and the small ^{14}N nuclear quadrupole coupling constants suggest that the NH_3 moiety continues to undergo large amplitude motions in the θ coordinate when bound to three Ne atoms. The experimental observation that this motion becomes more hindered as the number of Ne atoms in the cluster increases is supported by the topologies of the ab initio potential energy surfaces of the Ne_n−NH_3 (n = 1−3) family. The dynamics of

the Ar_n-NH_3 clusters do not adhere to the same trends, however, indicating that the identities of the Rg atom substituents continue to have a critical effect on the anisotropies of the potential energy surfaces for quaternary van der Waals complexes. The observation of two inversion tunneling states for the deuterated isotopomers of Ne_3-NH_3 supports minimum energy structures in which the C_3 axis of NH_3 is in the *ac*-plane of the complex, lying parallel to the plane of the Ne_3 ring. This is supported by the ab initio potential energy surfaces of Ne_3-NH_3 which show little dependence on the NH_3 monomer geometry at this orientation. Comparison of the inversion tunneling splittings in the deuterated Rg_n-NH_3 ($n = 1-3$) species provides evidence of subtle differences in the inversion dynamics of NH_3 as a function of the Rg cluster environment. Since the observed spectra are sensitive reflections of the topologies of the potential energy surfaces, the precise measurement of the small inversion tunneling splittings is crucial to the development of accurate intermolecular interaction potentials that include intramolecular modes such as NH_3 inversion. These interaction potentials are, in turn, fundamental to the goal of achieving a thorough understanding of solvation on a macroscopic level.

Acknowledgment. This work was funded by the Natural Sciences and Engineering Research Council (NSERC) of Canada. J.V. thanks NSERC and the University of Alberta for graduate scholarships.

Supporting Information Available: Tables of rotational transition frequencies for all isotopomers and ab initio data. This material is available free of charge via the Internet at http://pubs.acs.org.

JA035252P